Available online at www.sciencedirect.com
SCIENCE DIRECT
Polymer 46 (2005) 10908–10918
polymer
www.elsevier.com/locate/polymer

Measuring the extent of exfoliation in polymer/clay nanocomposites using real-time process monitoring methods☆

Anthony J. Bur*, Yu-Hsin Lee, Steven C. Roth, Paul R. Start

Materials Science and Engineering Laboratory, National Institute of Standards and Technology, Gaithersburg, MD 20899, USA

Received 29 April 2005; received in revised form 9 August 2005; accepted 30 August 2005
Available online 23 September 2005

Abstract

Dielectric and optical transmission measurements obtained during processing of polymer/clay composites yielded quantitative information about the extent of clay exfoliation in the polymer matrix. Measurements were made using an instrumented slit die that was situated at the exit of a twin screw extruder. Nylon 6, 11 and 12 resins were compounded with several organo modified montmorillonite clays. Dielectric and optical data were correlated with off-line transmission electron microscopy. Dielectric observations revealed a large Maxwell–Wagner (MW) relaxation whose characteristic frequency reflects an *RC* time constant associated with the conduction of ions and the polarization of the resin/clay interface. Optical transmission measurements showed that transmission increased with increasing extent of exfoliation because light scattering due to aggregate clay particles is reduced as the particles exfoliate nanosize silicate flakes. Extent of exfoliation models, based on MW relaxation time and its relationship to interfacial polarization, and based on optical transmission measurements, are developed.

Keywords: Polymer nanocomposites; Clay exfoliation; Nylon

1. Introduction

The purpose of compounding clays with polymer resins is to produce enhanced product performance with a relatively small amount of filler material. A large amount of published work in this area over the past decade demonstrates the benefits of compounding polymer with clay, namely, improvement in mechanical properties, barrier resin behavior and fire retardation properties [1–8]. Enhanced performance is a result of exfoliation of nano-size silicate flakes from larger aggregate particles that greatly increases the surface area of interaction between clay and resin. Measuring the amount of exfoliation that occurs during compounding of clay with the polymer resin is a prerequisite to establishing a knowledge base of nanocomposite materials properties and their functional relationship to the extent of exfoliation. The current practice for measuring the extent of exfoliation employs post-processing examination using transmission electron microscopy (TEM) and determining the number of exfoliated flakes per unit area. This involves counting the number of silicate flakes in a small area of the micrograph, e.g. 1 μm^2, and assuming that that number is characteristic of the entire extruded lot [1]. The technique is labor intensive and does not lend itself to monitoring the amount of exfoliation during compounding. Consequently, a vast area of parameter space, materials properties as a function of extent of exfoliation, remains unexplored. The functional relationships and scaling factors of material behavior with respect to the amount or extent of exfoliation remain unknown. This situation has greatly impeded advances in our understanding of clay nanocomposite performance and compromised the industrial and commercial applications of nanocomposite materials. In this paper, we present results of two measurements, dielectric spectroscopy and optical transmission, which are the basis for models that yield values for the extent of exfoliation. Our approach is to use these techniques to monitor the compounding of clay and polymer in real-time thereby establishing the means for controlling the amount of exfoliation during processing.

Our previously published work in the area of polymer/clay nanocomposites concentrated on the development of an on-line sensing device to monitor nanocomposite compounding using dielectric spectroscopy, optical transmission and fluorescence spectroscopy [9], and on real-time characterization of nylon/clay composites during compounding [10–14].

☆Contribution of the National Institute of Standards and Technology, not subject to copyright in the United States.

* Corresponding author. Tel.: +1 301 975 6748.
E-mail address: abur@nist.gov (A.J. Bur).

0032-3861/$ - see front matter © 2005 Elsevier Ltd. All rights reserved.
doi:10.1016/j.polymer.2005.08.091

2. Experimental procedures [15]

Three nylon resins, nylon 11 (Rilsan BESNO from Altofina), nylon 6 (Capron 8200 from Honeywell), and nylon 12 (Grilamide L16 natural from EMS Chemie) were used. Nylon 11 is a moderate viscosity extrusion grade resin with melting point at 185 °C, nylon 6 is a low viscosity resin with melting point at 225 °C, and nylon 12 is a low viscosity resin with melting point of 178 °C. Resins were compounded with four Cloisite clays from Southern Clay products designated as Na+, 15A, 20A, and 30B. The Na+ clay is natural clay containing no organo surfactant and the other three clays are organo modified clays that are derived from the natural clay using an ion exchange process. 15A and 20A are both prepared by ion exchange of naturally occurring sodium with quaternary ammonium (dimethyl, dihydrogenatedtallow) ion. The only difference between 15A and 20A is their surfactant concentration, which is 1.35 cation exchange capacity (CEC) and 1.03 CEC for 15A and 20A, respectively. Similarly, 30B is produced by ion exchange for a methyl, tallow, bis-2-hydroxyethyl quaternary ammonium ion. 30B differs from 15A and 20A not only by the surfactant functionality, which is polar for 30B and non-polar for 15A and 20A but also by the surfactant content, which is much lower for 30B (0.95 CEC). The powdered clay was compounded with the nylon resins at 4% mass fraction of clay in the resin. Prior to compounding both resin and clay were dried overnight at 80 °C in a vacuum oven. Compounding was carried out at 30 rpm using an 18 mm Haake Rheocord model 9000 co-rotating twin screw extruder.

The sensing device, called a dielectric slit die (Chemical ElectroPhysics), is mounted at the exit of a twin screw extruder and consists of a slit die that serves as a platform for mounting a variety of sensors. The slit, with dimensions of 28 mm wide by 2 mm high and 14.5 cm long, contains the dielectric sensor with interdigitating electrodes on one of its surfaces. When a voltage of 1 V_{rms} is applied across the electrodes, the in-phase and out-of-phase current is determined using a computer-controlled lock-in amplifier, (Stanford Research model SR810) which, in conjunction with instrument software, operates as a dielectric spectrometer (Chemical ElectroPhysics Proceptor). Complex relative permittivity, $\varepsilon^* = \varepsilon' - i\varepsilon''$, at 15 discrete frequencies in the range from 50 to 10^5 Hz was measured. A heating jacket surrounds the slit die, and temperature is controlled using a thermocouple inserted into the steel housing.

The optical fiber sensor is designed for insertion into a standard sensor port machined into the stainless steel housing of the slit die. We use an incoherent light source, a xenon arc lamp, with a 10 nm bandpass filter centered at 570 nm. The sensor consists of a bundle of seven 200 μm core optical fibers that are placed into a sleeved sensor bolt with a sapphire window at its end. When operating in the reflection mode, one of the fibers transmits light from the light source through a focusing lens, the sapphire window, the flowing resin composite, reflects off the opposite stainless steel wall of the slit, and reverses its path through the material, sapphire window and lens. The reflected light is collected by the other six fibers and is transmitted to the photomultiplier (PMT #2) detector. The intensity of the light source is monitored with another PMT (#1). The two light intensities are measured using a Stanford Research SR400 photon counter, and the ratio of the two light intensities, PMT #2 to PMT #1 or I/I_0, is a measure of the light transmission through the resin. More details about design and operation of the dielectric and optical sensors are available from a previous paper [9].

In addition to on-line dielectric and optical transmission measurements, off-line transmission electron microscopy (TEM) and dielectric measurements were carried out. Off-line dielectric measurements were made on the neat nylon resins and their composites in the semi-crystalline state. The samples were obtained from the twin screw extruded batch, pressed into disks (using the same temperature as for extrusion) that were 1 mm thick. Aluminum electrodes 2.54 cm in diameter were vacuum deposited on the disks. Measurements were made isothermally in 5 °C increments and in 0.2 logarithmic steps in frequency over a temperature range from −50 to 100 °C. Measurements were carried out over a frequency range from 20 Hz to 1 MHz using a precision LCR meter (HP 4284A) with application of 1 V_{rms}. The samples were kept under dry nitrogen gas during the measurement. As described below, our interest in the off line dielectric measurements was the temperature dependence of the γ relaxation in the nylons.

For measurements of the complex relative dielectric permittivity, $\varepsilon^* = \varepsilon' - i\varepsilon''$, the relative standard uncertainty of the on-line measurements, obtained from five measurements on the same sample, is 1% for ε' and 0.5% for ε'', and for off-line dielectric measurements it is 0.5% for ε' and 0.5% or 0.0005 whichever is larger for ε''. Standard uncertainty of the on-line temperature measurements is 1 °C, and for off-line measurements it is 0.2 °C. Relative standard uncertainty in the light transmission measurements is 0.15%. Uncertainties listed in Tables 1 and 2 (below) are standard deviations calculated from measurements of four to six different samples of the same composition.

Table 1
Dynamic relaxation parameters derived from curve fitting

	Log f_α (Hz)	Log f_{MW} (Hz)	δ_{MW}
At 198 °C			
Nylon 11	2.48	–	
Nylon 11/Na+	2.51	0.74	0.52
Nylon 11/20A	2.52	0.33	0.52
Nylon 11/15A	2.55	0.16	0.51
Nylon 11/30B	2.48	0.62	0.52
At 242 °C			
Nylon 6	2.35	–	
Nylon 6/20A	2.41	1.50	0.30
Nylon 6/15A	2.53	1.60	0.16
Nylon 6/30B	2.65	1.00	0.32
At 195 °C			
Nylon 12	2.33	–	
Nylon 12/20A	2.62	2.05	0.075
Nylon 12/15A	2.74	2.12	0.06
Nylon 12/30B	2.43	1.97	0.17

Table 2
Other relaxation parameters derived from curve fitting

	$\sigma\times10^3$ (S/m)	$\Delta\varepsilon_\alpha$	$\Delta\varepsilon_{MW}$	δ_α	ε_{inf}
At 198 °C					
Nylon 11	0.55±0.03	757±64	–	0.065±0.007	25.3±0.6
Nylon 11/Na+	1.54±0.02	2667±88	3175±65	0.059±0.005	23.2±0.8
Nylon 11/20A	1.01±0.02	1080±140	4745±252	0.028±0.013	11.6±1
Nylon 11/15A	1.23±0.05	2312±515	9662±1082	0.070±0.009	25.7±3
Nylon 11/30B	1.11±0.03	2146±86	3350±361	0.075±0.005	19.3±0.7
At 242 °C					
Nylon 6	0.314±0.01	315±87	–	0.16±0.03	32.2±0.4
Nylon 6/20A	1.39±0.06	6406±646	15877±3033	0.121±0.003	44.9±3
Nylon 6/15A	1.43±0.02	10670±316	18065±770	0.155±0.02	43.8±0.7
Nylon 6/30B	1.34±0.2	3170±658	16423±1823	0.205±0.05	55.3±3
At 195 °C					
Nylon 12	0.035±0.001	74±9	–	0.160±0.03	20.1±0.1
Nylon 12/20A	0.587±0.01	600±130	7780±1028	0.112±0.04	19.6±0.1
Nylon 12/15A	0.572±0.03	2270±882	16585±1937	0.121±0.005	17.0±0.5
Nylon 12/30B	0.409±0.02	1651±527	8490±794	0.035±0.012	18.0±1

3. Results and discussion

Fig. 1 shows real-time dielectric data for extrusion of nylon 11 compounded at 198 °C and 30 rpm with 4% mass fraction of organo modified 20A, 15A and 30B clays in the resin. Na+ clay was also compounded with polymer resin but yielded no exfoliation. Relative permittivity ε' and dielectric loss ε'' are plotted versus time for 15 frequencies ranging from 50 Hz to 100 kHz. Dielectric sensing started with the neat polymer at $t=0$ s. After extruding the neat polymer for 1580 s, nylon 11 with 4% mass fraction of 20A clay was added to the feeder. After a transition time extending from 1580 to 2270 s, the steady state dielectric properties of the nylon 11/20A clay were observed. In the continuation of the experiment, 4% mass fraction of 15A and 30B clays were added at $t=4000$ and 6700 s as indicated in the Fig. 1. These data for nylon 11/clay compounding are typical of the on-line dielectric data that was obtained for the nylon 6 and nylon 12 compounding that was carried out at 30 rpm and at 240 and 195 °C, respectively. The common characteristic of these data is that, for high processing temperatures, ionic conductivity dominates the low frequency dielectric behavior.

We see that the magnitude of the dielectric dispersion (the difference in relative permittivity between low and high frequencies) is greater for the clay/polymer nanocomposite than that for the neat polymer. This is because the introduction of the clay particles to the resin introduces ionic species that contribute to conductivity and polarization over and above that which is present in the neat resin. At processing temperatures, ion dissociation permits the surfactant ions to be the dominant charge carrier of current. The general features of the data in Fig. 1 are typical of the observations that we made for all nylon/clay composites, namely a large dispersion highlighted by increases in permittivity upon the addition of ion bearing clays due to electrode polarization and large dielectric loss at low frequency due to ion Dc conductivity. When plotted versus frequency, no apparent maximum is seen in the loss data, but curve fitting analysis (as described below) yields relaxation dispersions.

The protocol for analyzing these data taking into account electrical impedance due to electrode polarization and effects due to Dc conductivity has been described in previous publications [9–14]. For materials containing high concentrations of conducting ions, we consider that the measurement is that of a sample admittance in series with an electrode admittance [9,16]. The frequency behavior of the sample admittance is described by the Cole–Cole relaxation function [17]

$$\varepsilon^* = \varepsilon' - i\varepsilon'' = -\frac{i\sigma_{Dc}}{\omega\varepsilon_0} + \varepsilon_\infty + \sum_j \frac{(\Delta\varepsilon)_j}{\left[1+(i\omega\tau_j)^{1-\delta_j}\right]} \quad (1)$$

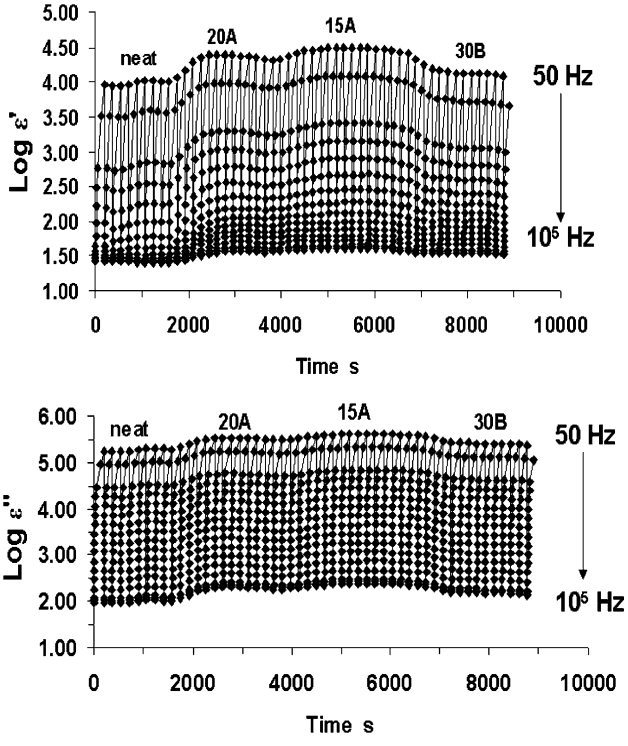

Fig. 1. Real-time relative permittivity and dielectric loss measurements for nylon 11 compounded with 20A, 15A and 30B clays at 198 °C.

where ε^* is the complex relative permittivity, ω is radial frequency, ε_0 is the permittivity of free space, $(\Delta\varepsilon)_j$ is the intensity of the jth relaxation, ε_∞ is the limiting relative permittivity at high frequency, τ_j is the characteristic relaxation time of the jth relaxation, and δ_j is a factor that describes the distribution of relaxation times for the jth relaxation process. The goal of the data analysis is to extract sample capacitance, conductance and conductivity, $C_s(\omega)$, $G_s(\omega)$ and σ_{Dc}, respectively, from the bulk measured admittance. For the highly conducting nylons in the melt, charge accumulation at the electrode is modeled as a capacitance/resistance admittance that is in series with the sample. The electrode polarization admittance in series with a Cole–Cole behaving material is what is measured and the curve fitting is designed to retrieve the parameters of the Cole–Cole equation. The electrode admittance is mostly capacitive in its behavior so that its presence mostly affects the measurement of ε', and its impact on ε'' is small but significant.

Between the electrode and sample admittances, there are seven fitting parameters to consider: $(\Delta\varepsilon)_j$, ε_∞, τ_j, δ_j, σ_{Dc}, C_{el}, and G_{el} where C_{el} and G_{el} are the capacitance and conductance of the electrode admittance. In setting initial values we consider the physics of the experiment and we note that all seven parameters are not of equal importance. There are three major parameters, $(\Delta\varepsilon)_j$, τ_j, and σ_{Dc}, whose initial values must be judiciously chosen in order to achieve a successful fit. For a highly conducting material, a good initial value of σ_{Dc} is easily obtained from the measured ε'' versus frequency curve by assuming that σ_{Dc} has a $1/\omega$ dependence. Once this estimated σ_{Dc} is subtracted from ε'', approximate initial values for $(\Delta\varepsilon)_j$ and τ_j will emerge. We have demonstrated this procedure in a previous paper [14]. Generally, the raw data will be the source of good initial values. An estimate for an initial value of ε_∞ can be obtained from the high frequency data and δ_j can be given a value of 0.2 which is typical of polymer behavior. The first non-linear fitting is carried out using the ε'' data alone because these are nearly independent of C_{el} and G_{el}. From this curve fitting, new initial values are obtained and used in a second curve fitting exercise where both ε' and ε'' are fit simultaneously. Also, with regard to the γ relaxation dynamics for nylon 6, 11 and 12 in the solid state, we rely on published literature to obtain good initial values. For example, the off-line log f versus $1/T$ roadmap for the relaxations in these polymers is available from a number of sources and we used the published data to place constraints on the initial values [18–36]. Relaxations with characteristic frequencies that were outside the experimental range were included in the curve fitting process if their characteristic frequency was within two decades of the experimental frequency limit. For the off-line measurements, outlying relaxations were easily identified by extrapolation of the log frequency versus reciprocal temperature plot.

The criterion for a good fit to the data is that curve fitting error be less than or equivalent to the uncertainty in the data. Curve fitting errors (square root of the square of the difference between data and fit) for the on-line measurements were between 0.3 and 0.8% and for the off-line measurements they were between 0.1 and 0.6%. The fact that these errors are less than the uncertainty in the data is attributed to a slightly smaller uncertainty than that stated above for data at frequencies greater than 5 kHz.

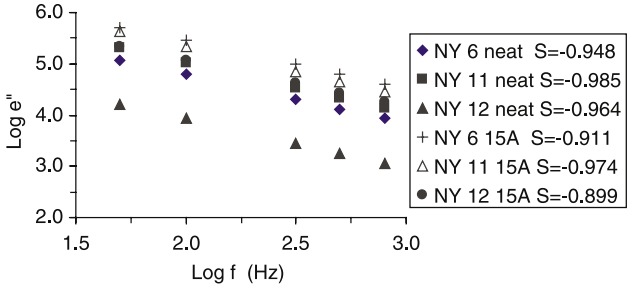

Fig. 2. Log ε'' versus log f for the neat nylons and the nylons compounded with 15A clay. S is the slope of the curves. Nylon 6 was compounded at 240 °C. Nylon 11 and 12 were compounded at 198 and 195 °C, respectively.

At processing temperatures and at low frequencies, σ_{Dc} contributes significantly to ε'' as frequency decreases due to its $1/\omega$ dependence. If ε'' is solely due to Dc conductivity, then the slope of log ε'' versus log frequency is -1. Using this criterion, conductivity data are plotted in Fig. 2 for neat nylon and the nylons with 15A clay. We note that the absolute value of all slopes S, neat polymers as well as clay composites, is less than one. (This holds true for the 20A and 30B composites as well, but the data are not plotted here in order to avoid crowding.) The implication is that, in addition to loss due to Dc conductivity, data in the low frequency regime include relaxation terms of Eq. (1).

The results of non-linear curve fitting using Eq. (1) in conjunction with an electrode admittance and Dc conductivity are shown in Figs. 3–7 where we have plotted relative permittivity ε' and dielectric loss ε'' versus log frequency for neat nylon 12 and several nylon/clay composites at their processing temperatures. In each case, large conductivity contributions to the dielectric loss have been subtracted from the measured loss to retrieve the dielectric relaxations. The three nylons were compounded with four clays, i.e. a total of 12 samples that were analyzed. The curve fitting results are tabulated in Tables 1 and 2 where Table 1 contains the dynamic data used in the model calculations of extent of exfoliation (below), and Table 2 contains the other relaxation parameters obtained from curve fitting. In the case of the neat resins, only one relaxation was observed, the α relaxation that is associated with macromolecular segmental motion at temperatures above the glass transition temperature. In the composites, two relaxations were observed, the α relaxation and a Maxwell–Wagner (MW) relaxation that is associated with the transport of ions through the resin matrix and the accumulation of those ions at the resin/clay interface [37,38]. The MW relaxation was identified by the magnitude of its intensity, $\Delta\varepsilon_{MW}$, which is much greater than that for the α relaxation. In semi-crystalline nylons, MW relaxations associated with the amorphous/crystalline interface have been observed by others [29,30], but we do not observe it in the neat melt amorphous state as

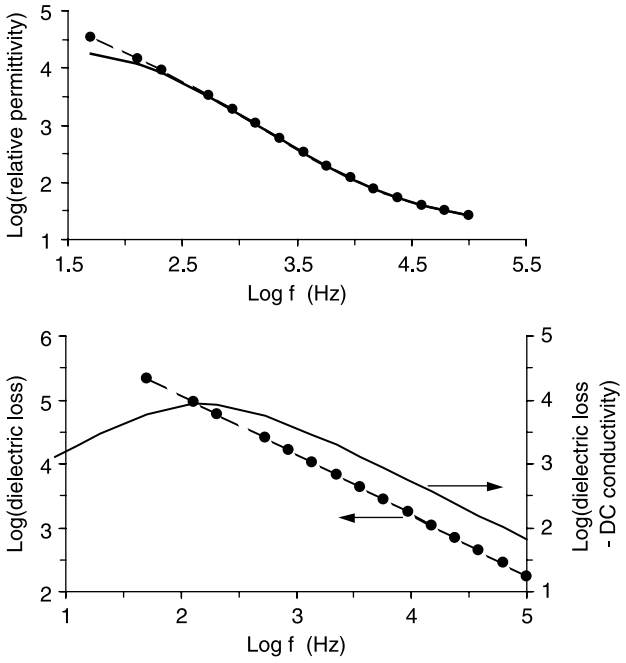

Fig. 3. Log ε' and Log ε'' versus Log f for NY12 15A at 195 °C. The points are the measured data. The dashed line is the fit to the data assuming an electrode admittance in series with the sample retrieved from the curve fitting algorithm using two relaxations with characteristic frequencies at $\log f = 2.12$ (Hz) and $\log f = 2.71$ (Hz), the MW and α relaxation, respectively. The solid lines are the relative permittivity ε' and the dielectric loss minus Dc conductivity (ε'') of the sample. The average error of the curve fit with respect to the data (ε' and ε'') is 0.35%.

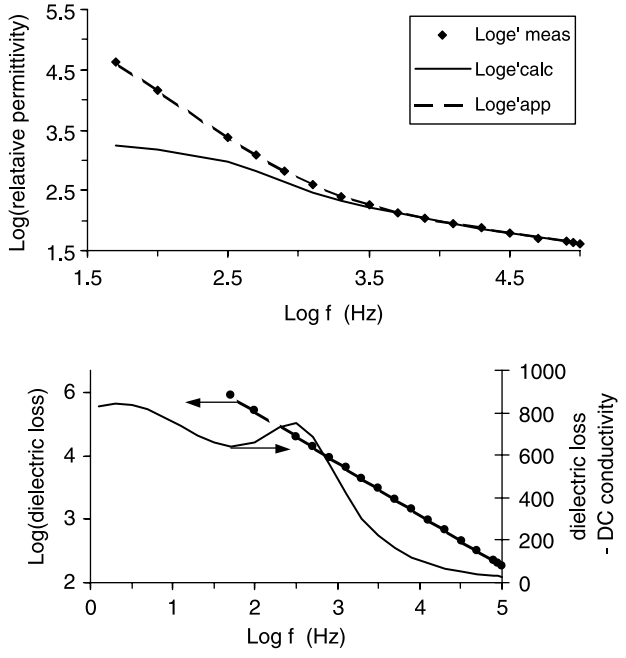

Fig. 4. Log relative permittivity ε' and Log dielectric loss ε'' versus Log f for nylon 11/20A at 198 °C. The points are the measured data. The dashed line is the fit to the data assuming an electrode admittance in series with the sample retrieved from the curve fitting algorithm using two relaxations with characteristic frequencies at $\log f = 0.31$ (Hz) and $\log f = 2.55$ (Hz), the MW and α relaxation, respectively. The solid lines are the relative permittivity ε' and the dielectric loss minus Dc conductivity (ε'') of the sample. The average error of the curve fit with respect to the data (ε' and ε'') is 0.48%.

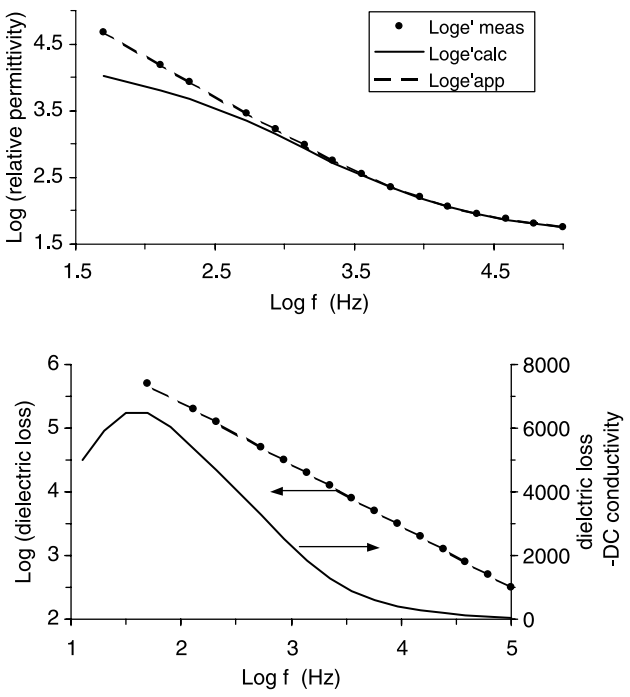

Fig. 5. Log relative permittivity ε' and Log dielectric loss ε'' versus Log f for nylon 6/15A at 242 °C. The points are the measured data. The dashed line is the fit to the data assuming an electrode admittance in series with the sample retrieved from the curve fitting algorithm using two relaxations with characteristic frequencies at $\log f = 1.53$ (Hz) and $\log f = 2.54$ (Hz), the MW and α relaxation, respectively. The solid lines are the relative permittivity and the dielectric loss minus Dc conductivity of the sample. The average error of the curve fit with respect to the data (ε' and ε'') is 0.33%.

there is no interface of contrasting dielectric constant to support polarization. In the discussion below, we will focus our attention on the dynamics of the MW relaxation in the melt composites and its relationship to the extent of exfoliation. The impact of exfoliation on other molecular dynamics, the α, β and γ relaxations, in both the melt and semi-crystalline state of the nylons is the topic of other publications from our laboratory [12,14].

The maximum standard uncertainty in the log frequency values of Table 1 is 0.05 and the maximum standard uncertainty in the values of δ_{MW} is 0.02. The uncertainties in the data of Tables 1 and 2 are not instrument uncertainties, but rather, they were obtained from the measurements on four to six different samples of the same composition and are associated with differences in the dielectric properties of the extruded material over the time of extrusion. The variations that we see in the dielectric data were also seen in the optical transmission measurements that are presented below.

Considering the MW relaxation in nylon 11 nanocomposites, we see that $\log f_{MW}$ varies from a high value of 0.74 for nylon 11/Na+ to a low value of 0.16 for the nylon 11/15A. Our interpretation is that f_{MW} is dependent upon the amount of exfoliated silicate particles and the size of the conducting surfactant ion. As exfoliation proceeds, nanosize silicate flakes present an ever expanding resin/silicate interface area that increases the internal capacitance of the composite where conducting ions can accumulate. Silicate flakes act as

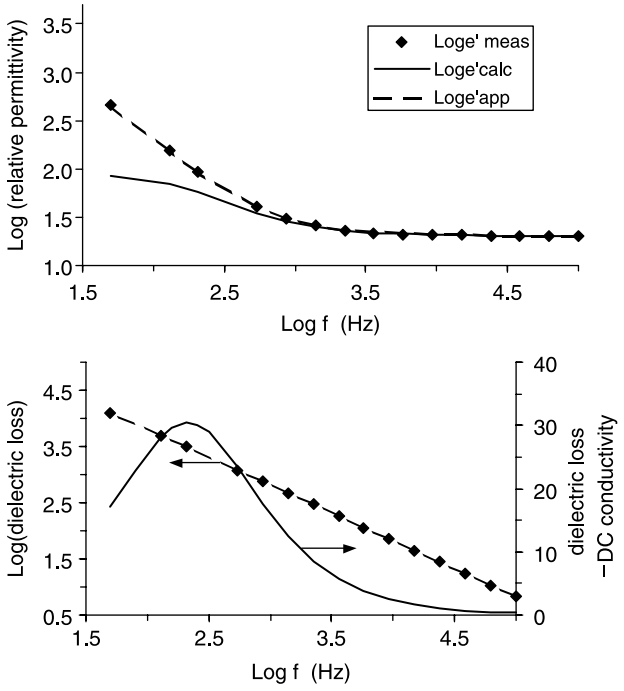

Fig. 6. Log relative permittivity ε' and Log dielectric loss ε'' versus Log f for neat nylon 12 at 195 °C. The points are the measured data. The dashed line is the fit to the data assuming an electrode admittance in series with the sample retrieved from the curve fitting algorithm using one relaxation with characteristic frequency at log $f=2.33$ (Hz), the α relaxation. The solid lines are the relative permittivity ε' and the dielectric loss minus Dc conductivity (ε'') of the sample. The average error of the curve fit with respect to the data (ε' and ε'') is 0.21%.

nanocapacitors in a sea of conductive resin, and as the capacitance increases with exfoliation the characteristic frequency of the MW relaxation decreases.

In general, the MW relaxation time $\tau_{MW}=(2\pi f_{MW})^{-1}$can be viewed as an electrical RC time constant where R is the resistance of the resin matrix and C the capacitance of the silicate particle. During exfoliation, R remains constant and τ_{MW} changes only through changes in C. We view the process as dissociated surfactant ions translating through the resin medium and accumulating at the surface of the silicate particle. For the model developed below, R is assumed to be constant for a constant temperature and independent of the amount of exfoliation.

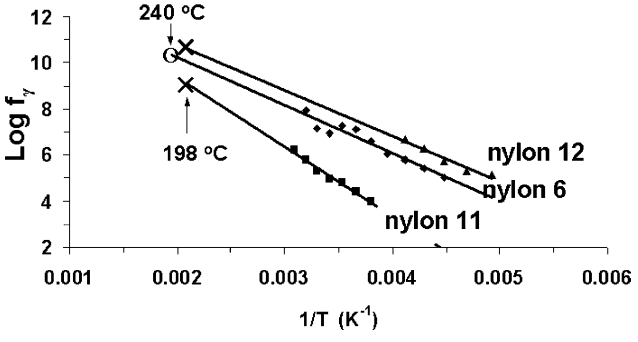

Fig. 7. The characteristic frequency of the γ relaxation for the three nylons is plotted versus reciprocal absolute temperature. X is terminus of extrapolation at 198 °C (nylon 11) and 195 °C (nylon 12), the processing temperature for nylon 11 and 12, and O is terminus of extrapolation at 240 °C, the processing temperature for nylon 6.

The dynamics are described as follows:

$$RC = \tau_{MW} \quad \text{or} \quad \rho\varepsilon = \tau_{MW} \tag{2}$$

where ρ is the resistivity of the resin and $\varepsilon=\varepsilon_0\varepsilon'_s$ is the permittivity of the silicate (ε'_s is its relative permittivity). Under the influence of an electric field E an ion with charge q will translate with a drift velocity v according to

$$bv = qE \tag{3}$$

where b is the translation friction constant. Assuming a spherically shaped ion, b is given by the Stokes frictional drag constant $b=6\pi\eta a$ where η is the viscosity of the resin melt and a is the radius of the spherical ion.

The ionic current density J is related to the field E through Ohm's law

$$J\rho = E \quad \text{or} \quad nqv\rho = E \tag{4}$$

where n is the number of ions per unit volume. Combining Eqs. (2)–(4) in conjunction with the definitions of b and ε we obtain

$$\varepsilon_0\varepsilon' = \frac{\tau_{MW}}{\rho} = \frac{nq^2\tau_{MW}}{6\pi\eta a} \tag{5}$$

where $\tau_{MW}=(2\pi f_{MW})^{-1}$. We will normalize Eq. (5) with respect to the number of ions n by multiplying both sides by the factor n_0/n where n_0 is a basis charge density whose value is arbitrarily set equal to 1 m^{-3}. This is permissible because the RC time constant depends on resistance and capacitance only and is independent of the number of charge carriers. We have

$$\frac{n_0\varepsilon'}{n} = \frac{n_0 C}{nC_0} = \frac{n_0 q^2\tau_{MW}}{6\pi\varepsilon_0\eta a} \tag{6}$$

where C is the effective capacitance of the silicate, C_0 is its vacuum capacitance and, by definition, $C/C_0=\varepsilon'$.

We note that the quantities on both sides of Eq. (6) are dimensionless and we define the quantity $n_0C/(nC_0)$ as the extent of exfoliation. The concept follows from our view of the silicate particle as a capacitor that changes in value as microstructure changes from aggregate to exfoliation. In this model, the aggregate particle has a low value of capacitance per surface area and the single exfoliated flake possesses the highest value per surface area. As exfoliation proceeds at a constant temperature, the resistance to ion conduction remains unchanged because the resistance is the drag force due to the resin viscosity, but the capacitance undergoes continuous change as each exfoliated flake presents a new surface to support polarization. Consequently, the RC time constant of Eq. (2) is controlled solely by the capacitance of the silicate in the aggregate, intercalated, or exfoliated state, or any combination thereof. Hundred percent exfoliation will have the highest capacitance, highest τ_{MW}, and lowest f_{MW}. On the other hand, values for the aggregate will be at the opposite extreme. In this manner, we can establish an exfoliation scale, anchored by these two extremes, by which the degree of exfoliation can be quantified.

Considering the right hand side of Eq. (6), we have $n_0 = 1\ m^{-3}$ and $q = 1.6\times10^{-19}$ C for singly charged ions ($q = 1$ C is used in the calculation). The radius a of the conducting ion is obtained from the X-ray measurement of the gallery spacing between silicate layers for each surfactant and is in the ratio Na+:30B:20A:15A equal to 1:5.0:8.35:8.35 [39]. For the 15A, 20A, and 30B surfactant ions, η is the micro or molecular level viscosity of the resin as it expresses drag on the translating ion. One must distinguish between micro and macro viscosity where the macro viscosity is the bulk viscosity that we measure using a pressure drop along the slit die and micro viscosity refers to effects due to the local molecular environment that a conducting ion experiences [40–43]. Micro viscosity can be obtained from a measurement of the rotational dielectric relaxation of a polar surfactant, such as 30B, in a resin matrix. Using the Stokes relationship for a sphere rotating in a viscous medium, the rotational relaxation time τ_r is

$$\tau_r = \frac{8\pi\eta a^3}{2kT} \tag{7}$$

where T is absolute temperature and k is Boltzman's constant. Eliminating η between Eqs. (6) and (7) yields

$$\frac{n_0 C}{nC_0} = \frac{2n_0 q^2 \tau_{MW} a^2}{3\varepsilon_0 kT\tau_r} \tag{8}$$

We have not yet obtained direct measurements of τ_r for the surfactant ion, but we will approximate its value by using the relaxation time of the γ dielectric relaxation process of the resin. This is a reasonable approximation considering that the γ relaxation arises from rotation of a small molecular dipole entity on the polymer chain. From off-line measurements as a function of temperature that were extrapolated to the processing temperature (Fig. 7), we obtained $\tau_r = 1.6\times10^{-10}$ s at 198 °C for nylon 11, and $\tau_r = 1.2\times10^{-11}$ s for nylon 6 at 240 °C, and $\tau_r = 4.5\times10^{-12}$ s for nylon 12 at 195 °C. Examples of off-line curve fitting are shown in Figs. 8–10.

Eq. (8) is further modified in order to account for the distribution of relaxation times that are expressed by the MW relaxation of each composite. The exponent, $1-\delta$, in the denominator of the Cole–Cole equation has values between 0 and 1 and is inversely proportional to the distribution of relaxation times. We propose that a narrow distribution of relaxation times, $\delta \approx 0$, reflects uniform microstructure. Thus, the ideal 100% exfoliated nanocomposite will have $1-\delta \approx 1$ expressing the relaxation behavior of silicate flake nano-capacitors that are uniform in size and shape. The extent of exfoliation becomes

$$\frac{n_0 C}{nC_0} = \frac{2n_0 q^2 \tau_{MW} a^2}{3\varepsilon_0 kT\tau_r}(1-\delta) \tag{9}$$

Fig. 11 is a linear scale of the extent of exfoliation, $n_0C/(nC_0)$, calculated using Eq. (9) and values from Table 1 for nylon 6, 11, 12 compounded with the clays. On this scale nylon 6/30B and nylon 11/15A composites have the highest extent of

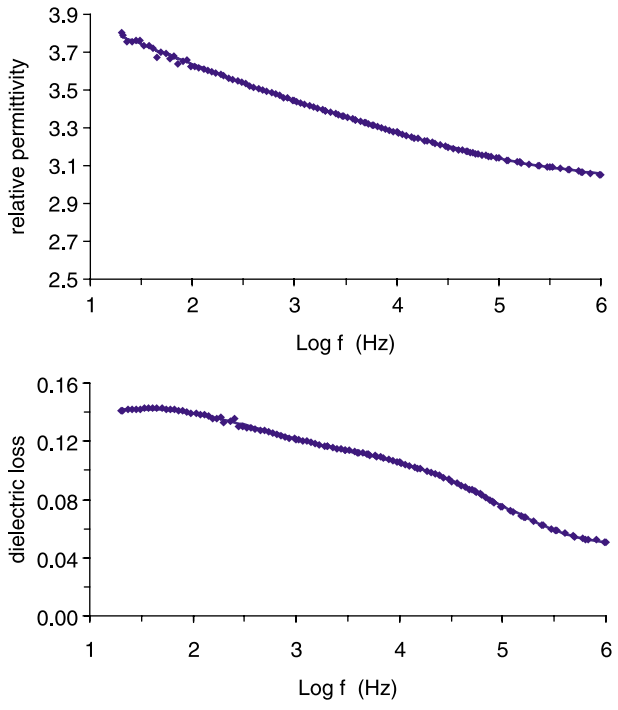

Fig. 8. Relative permittivity ε' and dielectric loss ε'' versus Log f for neat nylon 11 at 0 °C. Points are measured data. Solid lines (partially obscured by the data points) are the fits to the data taking into account three relaxations with characteristic frequencies at log $f = 1.39$ (Hz), log $f = 4.39$ (Hz) and log $f = 6.98$ (Hz), the β, γ, and δ relaxations, respectively. Since Dc conductivity is negligible, the dielectric loss of the material is as measured. The average curve fitting error for these data (both ε' and ε'') is 0.22%.

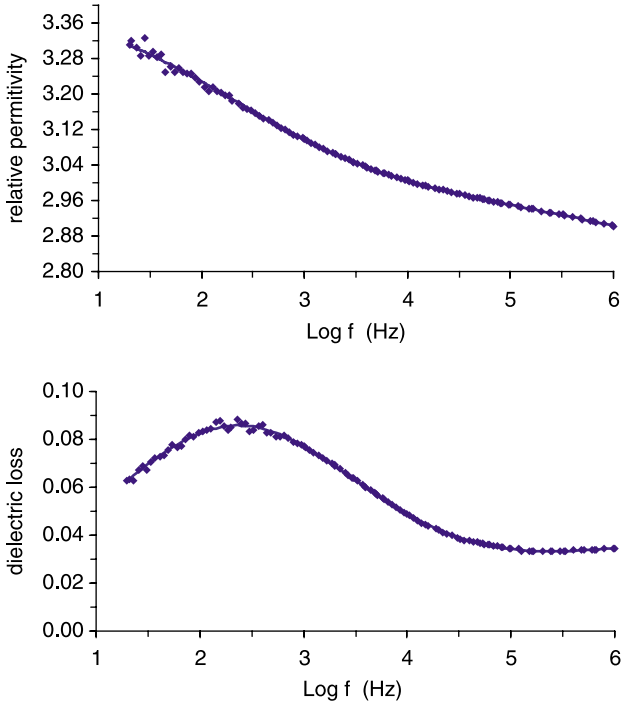

Fig. 9. Relative permittivity ε' and dielectric loss ε'' versus Log f for neat nylon 12 at −30 °C. Points are measured data. Solid lines (partially obscured by the data points) are the fits to the data taking into account three relaxations with characteristic frequencies at log $f = 2.33$ (Hz), log $f = 6.87$ (Hz) and log $f = 8.0$ (Hz), the β, γ, and δ relaxations, respectively. Since Dc conductivity is negligible, the dielectric loss of the material is as measured. The average curve fitting error for these data (both ε' and ε'') is 0.39%.

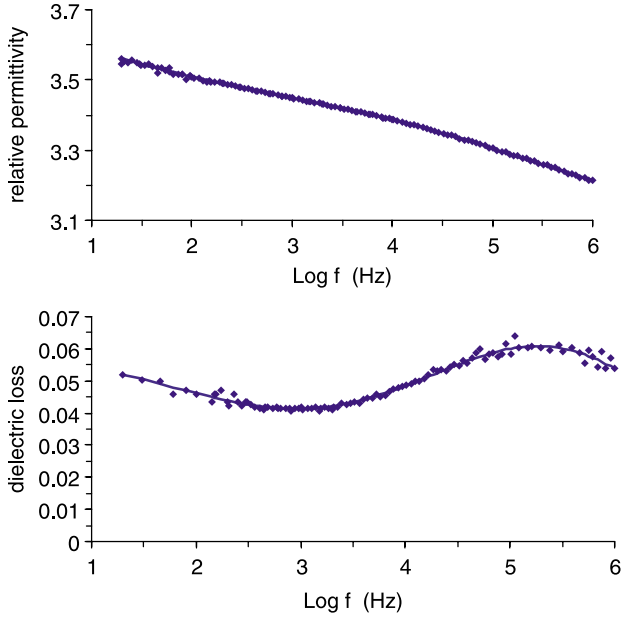

Fig. 10. Relative permittivity ε' and dielectric loss ε'' versus Log f for neat nylon 6 at −40 °C. Points are measured data. Solid lines (partially obscured by the data points) are the fits to the data taking into account two relaxations with characteristic frequencies at log f=0.585 (Hz) and log f=5.39 (Hz), the β and γ relaxations, respectively. Since Dc conductivity is negligible, the dielectric loss of the material is as measured. The average curve fitting error for these data (both ε' and ε'') is 0.62%.

exfoliation and Na+, which does not exfoliate, has the lowest value. A transmission electron micrograph (TEM) of the nylon 11/15A specimen is shown in Fig. 12. Similar TEMs were obtained for partially exfoliated nylon 6/30B, nylon 11/30B and nylon 11/20A composites. For nylon 12/30B, which has a low value on the extent of exfoliation scale, the TEM of Fig. 13 shows intercalated tactoids but very few exfoliated flakes.

3.1. Optical measurements

Optical transmission for nylon 11 compounded with the four clays is shown in Fig. 14. The graph is typical of optical transmission observations obtained for all of the nylon/clay compounding. The data show light transmission decreasing when the sodium clay is added and increasing above the Na+ clay value when exfoliated organo clays are compounded. Variations in the light transmission values observed in data for each clay composite are significant and are attributed to variations in the extent of exfoliation and to slight changes in the concentration of

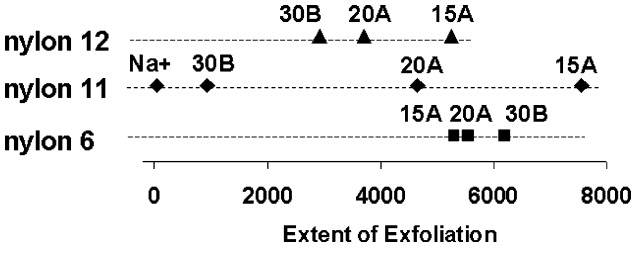

Fig. 11. Extent of exfoliation scale calculated from Eq. (10) for nylon 12, nylon 11 and nylon 6.

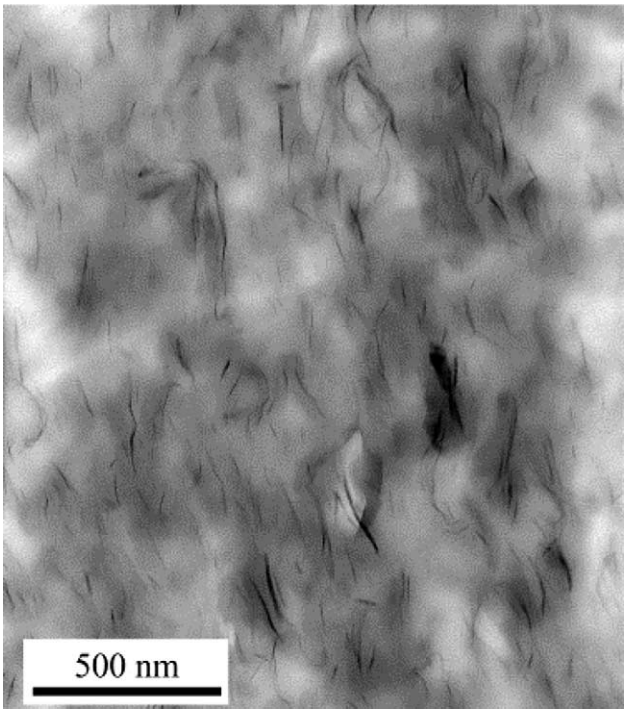

Fig. 12. TEM of nylon 11 compounded with 15A clay.

clay as the components are fed into the extruder. In the case of 20A clay, which was always compounded immediately after the Na+ clay, the data may be compromised by Na+ clay that had not been completely flushed from the slit channel. Light transmission values and dielectric data for 20A clay composites were taken from the end of the 20A run.

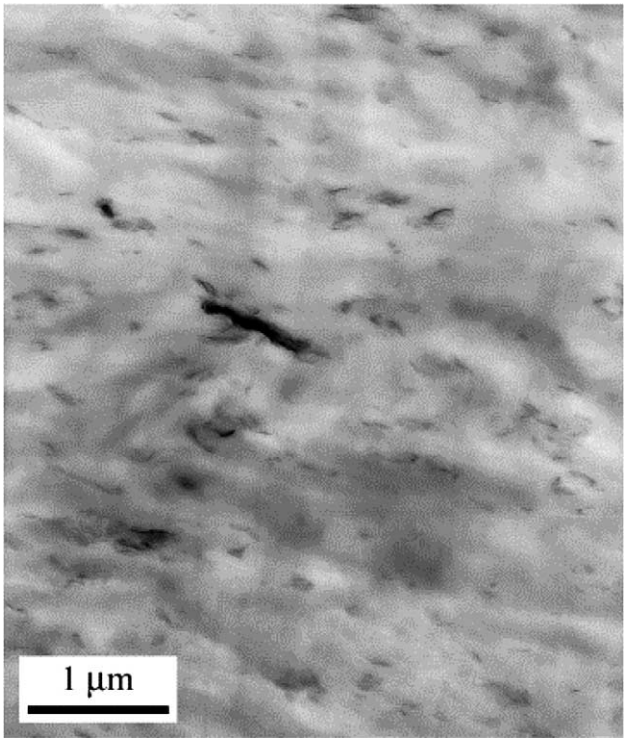

Fig. 13. TEM of nylon 12 compounded with 30B clay.

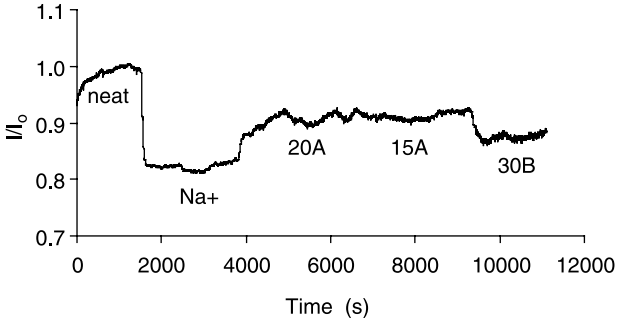

Fig. 14. Optical transmission for nylon 11 compounded with four clays at 198 °C.

The observed transmitted light through the composite is the result of light that has been attenuated by large aggregate clay particles that attenuate light by refractive and diffractive effects. Rayleigh light scattering from nano-size particles also occurs but the intensity of this scattering is negligible compared to that due to micron size clay particles. Large clay particles scatter light in proportion to the difference in polarizability between the nylon matrix and the clay particle. As exfoliation proceeds, nano-size flakes separate from the parent particle that decreases in size and scatters or attenuates less light. Both the neat polymer and an ideally 100% exfoliated nanocomposite will have approximately the same light transmission because neither specimen will contain particles with light refracting or diffracting capability.

We consider that light attenuation is described by a modified Beer's law. In our experiments, the optical path length is held constant by the dimensions of the slit so that the light attenuation function is normalized with respect to path length. Rather, the independent variable is the volume fraction φ of clay particles that attenuate/scatter light. We employ the concept of volume fraction of scatterers that follows from light scattering work of Stein and co-workers who studied light scattering from polymer crystal spherulites that were of the same size as the clay particles compounded in these nanocomposites [44–46]. We consider the function

$$I = I_0 e^{-\beta\varphi} \tag{10}$$

where I is the transmitted light, β is an attenuation coefficient proportional to the difference in polarizability between clay particles and the nylon matrix and φ is the volume fraction of aggregate clay particles that scatter light. φ remains small for our measurements, less than 3%, so that the quadratic term used by Stein can be neglected [45,46]. We recognize two boundaries: the neat polymer represents 0% aggregate or 100% exfoliated clay, and the Na+ composites are the opposite extreme, 100% aggregate with no exfoliation. Applying these boundaries in conjunction with our knowledge of the density of the clay [39], and the indices of refraction, we use Eq. (10) to express φ in terms of light transmission. Here we use index of refraction $n_n = 1.53$ for all three nylons with density $\rho = 1.0$ g/cm^3 at their processing temperatures, $n_{Na} = 1.677$ for Na+ clay with $\rho = 2.88$ g/cm^3, $n_{15A} = 1.415$ for 15A clay with $\rho = 1.66$ g/cm^3, $n_{20A} = 1.4285$ for 20A clay with $\rho = 1.77$ g/cm^3,

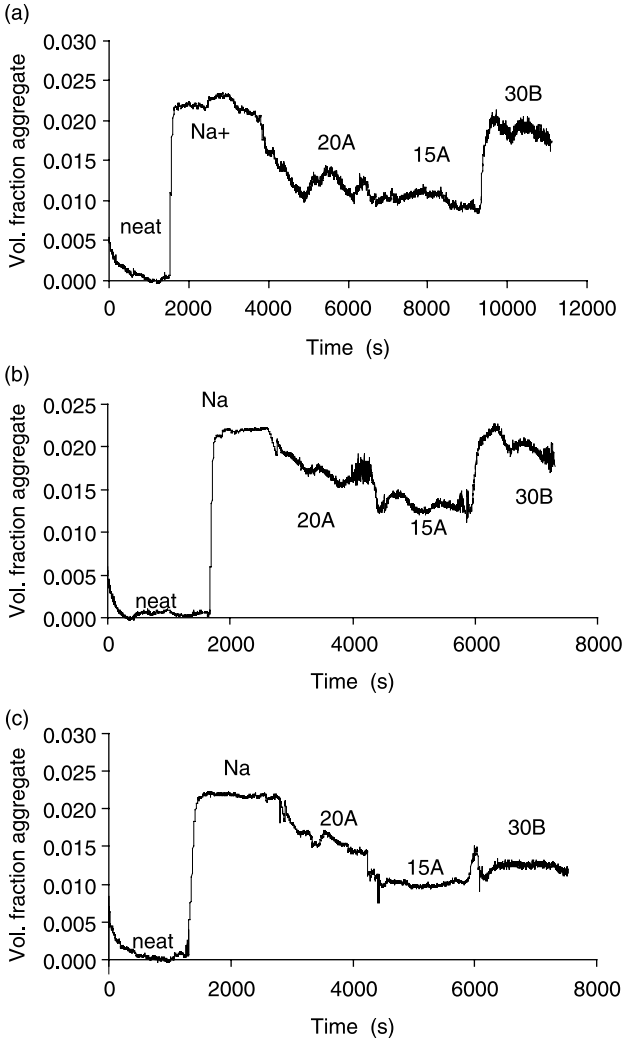

Fig. 15. Volume fraction of aggregate versus time for (a), (b) and (c): nylon 11, nylon 12 and nylon 6 compounded with clays.

and $n_{30B} = 1.447$ for 30B clay with $\rho = 1.98$ g/cm^3 [39,47–49]. These values of index of refraction were obtained from the cited literature and adjusted for small differences in density by using the Lorentz–Lorenz equation (LL). Also, LL was used to obtain indices of the organo clays by summing the polarizations from silicate and surfactant components [50].

Given that the differences between indices of refraction between clays and nylons are small, we assume, to a first approximation, that the attenuation coefficient β is a linear function of difference in polarizability between resin and clay, i.e. $\beta = K\Delta(n^2)$ where K is a constant of proportionality and $\Delta(n^2)$ is the difference in the square of index of refraction between resin and clay. A value of K was obtained from Eq. (10) using I/I_0 data for the nylon/Na+ clay composite (no exfoliation) for which we assign $\Delta(n^2) = (1.677)^2 - (1.53)^2$, and we assume that all of the clay is in the aggregate state, i.e. $\varphi_{Na} = 0.0155$ for 4% mass fraction of Na+ clay in the nylon. For presentation of results shown in Fig. 15 (a)–(c), φ_{Na} has been adjusted to equal 0.0222, which is the average volume fraction of the organo modified clays at 4% mass fraction of clay in resin, thus normalizing the difference in densities

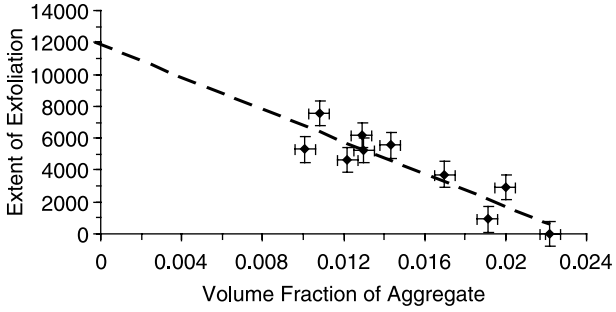

Fig. 16. Extent of exfoliation from dielectric measurements is plotted versus volume fraction aggregate from optical transmission measurements. Dashed line is a linear regression of data extrapolated to zero volume fraction of aggregate.

(and volume fraction) between the Na+ clay and the modified clays.

The plots of Fig. 15 are quantitative indicators of the extent of exfoliation that has occurred during processing. The volume fraction of aggregate that contributes to light attenuation reaches a minimum near 0.011 for nylon 11/15A and for nylon 6/15A and 30B composites, i.e. approximately half of the aggregate 15A and 30B clays have exfoliated. Examining the extent of exfoliation scales of Figs. 11 and 15, we note that the dynamic range of the dielectric scale is much broader than that of the light transmission. Not only are differences in exfoliation accentuated on the dielectric scale, but also it must be recognized that the two instruments measure different quantities and reflect exfoliation based on different physical principles. Light scattering is sensitive to the aggregate material that remains after silicate flakes have peeled off, but is not sensitive to single nano-flakes or small tactoids and groupings of silicate flakes that are too small to scatter light. On the other hand, the MW dielectric relaxation is sensitive to the nanosize flakes as their exfoliation presents interfacial surface area to the medium that determines the MW characteristic relaxation time. The increase in the extent of exfoliation in a given polymer is directly related to the product of the MW relaxation time and $(1-\delta)$. For different polymer systems this product is normalized by dividing by the temperature and the intrinsic dipolar rotational time of the neat polymer.

Fig. 16 is a plot of extent of exfoliation (dielectric) versus volume fraction of aggregate (optics) that shows the correlation between the two measurements. The correlation is evident, but there is scatter in the data that we attribute to the approximations that were made in the dielectric extent of exfoliation model, namely using the γ relaxation and its extrapolation on the temperature scale to calculate the micro-viscosity. A linear extrapolation to $\varphi=0$ of the data of Fig. 16, yields a value, 12,000, that one would expect for the dielectric extent of exfoliation for $\varphi=0$ or 100% exfoliation.

The measurements and concepts developed here open a window of opportunity for conveniently determining the extent of exfoliation without resorting to TEM measurements. The light transmission measurement is particularly convenient in concept and application. In the manufacturing environment, the raw data obtained from light transmission measurements, e.g. Fig. 14, can be used as a real-time, empirical guide to assess product extrusion. Continuous monitoring of light transmission during extrusion provides a continuous stream of data that allows for statistical analysis of the volume fraction of aggregate. As we mentioned above, the measurements provide the means to build a knowledge base of materials properties that depend on extent of exfoliation. It is now possible to determine the functional relationships and scaling factors between nanocomposite mechanical and engineering properties and extent of exfoliation. Also, the measuring capability is a prerequisite for controlling the extent of exfoliation in nanocomposites during processing. Controlling exfoliation in conjunction with an established database of materials properties versus extent of exfoliation will allow processors to target and predict product performance.

References

[1] Dennis HR, Hunter DL, Chang D, Kim S, White JL, Cho JW, et al. Polymer 2001;42:9513.
[2] Krishnamoorti R, Giannelis EP. Macromolecules 1997;30:4097.
[3] Fornes TD, Yoon PJ, Keskkula H, Paul DR. Polymer 2001;42:9929.
[4] Hasegawa N, Okamoto H, Kato M, Usuki A. J Appl Polym Sci 2000;78:1918.
[5] LeBaron PC, Wang Z, Pinnavaia TJ. Appl Clay Sci 1999;15:11.
[6] Strawhecker KE, Manias E. Chem Mater 2000;12:2943.
[7] Yang F, Ou Y, Yu Z. J Appl Polym Sci 1997;69:355.
[8] Zanetti M, Lomakin S, Camino G. Macromol Mater Eng 2000;279:1.
[9] Bur AJ, Roth SC, Lee YH, McBrearty M. Rev Sci Instrum 2004;75:1103.
[10] Bur AJ, Roth SC, Lee YH, Noda N, McBrearty M. Plast Rubber Compos 2004;33:5.
[11] Davis RD, Bur AJ, McBrearty M, Lee YH, Gilman JW, Start PR. Polymer 2004;45:6487.
[12] Lee YH, Bur AJ, Roth SC, Start PR. Macromolecules 2005;38:3828.
[13] Lee YH, Bur AJ, Roth SC, Start PR, Harris RH. Polym Adv Technol 2005;16:249.
[14] Noda N, Lee Y-H, Bur AJ, Prabu VM, Snyder CR, Roth SC, McBrearty M. Polymer 2005;46:7201.
[15] Identification of a commercial product is made only to facilitate experimental reproducibility and to describe adequately the experimental procedure In no case does it imply endorsement by NIST nor does it imply that it is necessarily the best product 2004.
[16] Pizzitutti F, Bruni F. Rev Sci Instrum 2001;72:2502.
[17] Cole RH. J Chem Phys 1955;23:493.
[18] Baker WO, Yager WA. J Am Chem Soc 1942;64:2171.
[19] Bizet A, Nakamura N, Teramoto Y, Hatakeyama T. Thermochim Acta 1994;237:147.
[20] Boutros S, Rizk HA, Hanna A, Gerges MK. J Chim Phys Phys- Chim Biol 1979;76:501.
[21] Boyd RH. J Chem Phys 1959;30:1276.
[22] Boyd RH, Porter CH. J Polym Sci, Part A-2 1972;10:647.
[23] Boyd RH. Polymer 1985;26:323.
[24] Chatain D, Gautier P, Lacabanne C. J Polym Sci, Polym Phys 1973;11:1631.
[25] Frank B, Frubing P, Pissis P. J Polym Sci, Part B: Polym Phys 1996;34:1853.
[26] Hanna AA. Thermochim Acta 1984;76:97.
[27] Ikeda S, Matsuda K. Jpn J Appl Phys 1980;19:855.
[28] Laredo E, Hernandez MC. J Polym Sci, Part B: Polym Phys 1997;35:2879.
[29] Laredo E, Grimau M, Sanchez F, Bello A. Macromolecules 2003;36:9840.
[30] McCall DW, Anderson EW. J Chem Phys 1960;32:237.

[31] Neagu RM, Neagu E, Kyritsis A, Pissis P. J Phys D: Appl Phys 2000;33:1921.
[32] Pathmanathan K, Johari GP. J Polym Sci, Part B: Polym Phys 1993;31:265.
[33] Pathmanathan K, Johari GP. J Chem Soc, Faraday Trans 1995;91:337.
[34] Russo P, Acierno D, Di Maio L, Demma G. Eur Polym J 1999;35:1261.
[35] Varlet J, Cavaille JY, Perez J, Johari GP. J Polym Sci, Part B: Polym Phys 1990;28:2691.
[36] Yemni T, Boyd RH. J Polym Sci, Part B: Polym Phys 1979;17:741.
[37] Maxwell JC. Electricity and magnetism. Oxford: Clarendon; 1892.
[38] Wagner KW. Arch Elektrotech 1914;2:371.
[39] Cloisite product specifications, Southern clay products, 2004, www.wcprod.com.
[40] Benamotz D, Drake JM. J Chem Phys 1988;89:1019.
[41] Fung BM, Mcgaughy TW. J Chem Phys 1976;65:2970.
[42] Meakins RJ. Trans Faraday Soc 1958;54:1160.
[43] Roy M, Doraiswamy S. J Chem Phys 1993;98:3213.
[44] Stein RS, Cronauer J, Zachmann HG. J Mol Struct 1996;383:19.
[45] Yoon DY, Stein RS. J Polym Sci Polym Phys 1974;12:735.
[46] Thomas CL, Bur AJ. Polym Eng Sci 1999;39:1291.
[47] Aharoni SM. n-Nylons: their synthesis, structure and properties. New York: Wiley; 1997.
[48] Babin M, Morel A, Fournier-Sicre V, Fell F, Stramski D. Limnol Oceanogr 2003;48:843.
[49] Schaerer AA, Busso CJ, Smith AE, Skinner LB. J Am Chem Soc 1955;77:2017.
[50] Handbook of chemistry and physics. Weast RC (Ed), Boca Raton, FL: CRC Press; 1986.